Modelling of the pulsatile blood flow in an arterial tree of retinal vasculature

Poo Balan GANESAN [1], Shuisheng HE [1,*], Heping XU [2]

* Corresponding author: Tel.: +44 (0)1224 272799; Email: s.he@abdn.ac.uk
1: School of Engineering, Aberdeen University, UK
2: School of Medicine, Aberdeen University, UK

Abstract The paper presents a numerical investigation of pulsatile blood flow in arterial vasculatures of a mouse retina using a Womersley model incorporating an appropriate outlet boundary impedance at the end of the terminal vessels of the arterial tree (pre-capillary arterioles). The mouse retinal flatmount was prepared for confocal microscopy and the morphometric information of the vasculature was obtained from the confocal images. The pulsatile analysis focused on one of the arterial trees in the retinal vasculature. We included the *in vivo* viscosity evaluated from the mathematical models of Fahraues-Lindquist effect and the plasma skimming effect in the microcirculation. Comparative investigations of the pulsatile circulation were carried out for cases of constant viscosity, *in vivo* viscosity, zero and non-zero outlet boundary impedance. In addition, the dependency of the oscillating input impedance at the inlet of the arterial trees on angular frequencies of the oscillation and vessel elasticises was also studied. The study shows the pulsatile blood flow prediction is largely influenced by the outlet boundary impedance. The oscillating input impedance at the inlet of the arterial tree is also found to be significantly dependent on the angular frequency and the Young modulus of the vessel segment.

Keywords: Retinal vasculature, Network model, Pulsatile blood flow, Womersley solution, Microcirculation.

1 Introduction

The blood flow in human retinal vessels is pulsatile, especially in retinal arteries (Feke *et al.*, 1987; White, 2003; Rao *et al.*, 2008). Pulsation is also reported in small arteriolar vessels (Riva and Petrig, 1980) and interestingly, in veins near the optic disc of the human retina (Levine, 1998; Balarathnasingam, 2007; Nicolela, 2007). Therefore, it is useful to study pulsatile blood flow in retinal vasculatures using a model that includes the morphometric data and the elasticity of the vasculature. This should lead to a better understanding of retinal blood flow under normal and pathological conditions.

The modelling of pulsatile blood flow in an elastic vessel is carried out using the mathematical model of Womersley's solution. The model was initially developed by Womersley and afterwards used by many other researchers, e.g., McDonalds (1960), Attinger (1964), Atabek (1966), Pedley (1980), Zamir (2005) and Olufen et al. (2000). The Womersley obtained a frequency domain based analytical solution, which is particularly useful for the evaluation of pulsatile blood flow in a large vascular network. The shortcoming of the model is that the nonlinear advective term in the momentum equation is neglected. However, in small vessels, the nonlinear losses are minor and linear models are adequate to describe flow velocity and pressure waves. In a recent application, Huo & Kassab (2006) found that the result of the pulsatile blood flow of the entire coronary arterial trees calculated from the Womersley analysis was in close agreement with experimental investigation.

The objective of the current work is to conduct a theoretical investigation of the pulsatile blood flow in an arterial tree of a mouse retinal vasculature using the Womersley analysis and incorporating an appropriate boundary condition at the end of pre-capillary arterioles and an *in vivo* effective viscosity. The pulsatile flow was generated by imposing a single harmonic pressure pulse at the inlet of the artery. Dynamic responses of the blood flow in various locations of the arterial network was studied for various conditions, including constant viscosity and *in*

vivo viscosity, zero and non-zero impedances at the terminals of pre-capillary arterioles. The dependency of the oscillating input impedance at the inlet of the arterial trees on angular frequencies and vessel elasticises was also investigated.

2 Methodology

2.1 Topology of the arterial trees and outlet boundary impedance

The morphometric information of retinal vasculature was obtained from confocal scanning microscopic images of mouse retinas that were prepared using flat-mount technique. The confocal images provided data on 3D distributions of the retinal vasculature. Using such morphometric information and a model of uniformly distributed capillary vasculatures, we built a detailed network model, which includes arterial, veinal and capillary vasculatures, to determine nodal pressure and segmental flowrate in the retinal network assuming a steady laminar flow with a constant viscosity (Ganesan *et al.*). The topologies of retina studied are given in Figure 1, in which the arterial trees are labelled A1 to A6. The vessels branch dichotomously before giving rise to capillary vasculatures.

The modelling of pulsatile blood flow to be reported here was carried out for the arterial tree A1 with boundary impedance specified at the terminal vessels of the arterial tree (end nodes of pre-capillary arterioles). The diameter of the vessel segments in A1 is ranged from 25 to 5.75μm. The boundary impedance info is obtained from the steady flow solution.

2.2 Mathematical model

The mathematical formulation used is based on the Womersley solution of pulsatile flow in an elastics vessel. The detailed formulation can be found in Mette *et al.* (2000) and Huo and Kassab (2006). Briefly, the equations of the conservation of mass and momentum are one dimensional (1D), linear, unsteady and axisymmetric. The non-linear advection term in the momentum equation is neglected as a first approximation for the pulsatile blood flow. The validity of the approximation has been shown to be reasonable especially in a small vessel in which viscous effects overweighs the inertia effects. A linear constitutive equation is used that relates the cross-sectional area (or radial deformation) of an elastic vessel to pressure.

Flow and pressure are assumed periodic and the governing equations are solved analytically in the form of Bessel function. This solution provides a frequency-dependent relationship between the pressure (P) and flow (Q) in the form of an impedance ($Z=P/Q$), which is the resistance of the flow. The input impedance of a vessel segment, $Z(0,\omega)$ is given as a function of the outlet impedance, $Z(L,\omega)$ as

$$Z(0,\omega)=\frac{ig^{-1}\sin(\omega L/c)+Z(L,\omega)\cos(\omega L/c)}{\cos(\omega L/c)+igZ(L,\omega)\sin(\omega L/c)} \tag{1}$$

where a and b are constants of integration, L is the length of vessel segment, the parameter g and the wave propagation velocity c are given as

$$g=\sqrt{CA_0(1-F_J)/\rho} \tag{2}$$

$$c=\sqrt{\frac{A_0(1-F_J)}{\rho C}} \tag{3}$$

$$\text{with, } F_J=\frac{2J_1(w_0)}{w_0J_0(w_0)} \tag{4}$$

where, $w_0^2=i^3w^2$ ($w^2=r_0^2\omega/\nu$ is the Womersley number) and $J_0(x)$ and $J_1(x)$ are the zeroth and first order Bessel functions. The compliance, C is approximated as

$$C\approx\frac{3A_0a}{2Eh} \tag{5}$$

where, A_0 is the cross-sectional area at diastolic pressure, a is the vessel segment radius, E is the Young's modulus (strain independent) and h is the wall thickness of vessel segment.

2.3 *In vivo* viscosity

The viscosity in the vessel segments was evaluated based on the mathematical model of *Pries et al.* (1994) which is expressed as

$$\frac{\eta_{vivo}}{\eta}=\left[1+\left(\frac{\eta_{0.45}}{\eta}-1\right)\frac{(1-H_D)^C-1}{(1-0.45)^C-1}\right]\left(\frac{D}{D-1.1}\right)^2 \quad (6)$$

$$\frac{\eta_{0.45}}{\eta}=6\cdot e^{-0.085D}+3.2-2.44\cdot e^{-0.06D^{0.645}} \quad (7)$$

where D, HD, η_{vivo}, $\eta_{0.45}$, η are the diameter, the hematocrit, the effective *in vivo* viscosity, the effective viscosity of blood with 45 per cent of *HD* and the viscosity of suspending medium, respectively. The parameter C is expressed as

$$C=\left(0.8+e^{-0.075D}\right)\left(-1+\frac{1}{1+10^{-11}D^{12}}\right)+\frac{1}{1+10^{-11}D^{12}} \quad (8)$$

Hematocrit computation; The uneven distribution of erythrocytes into daughter vessels, which determines *HD* in a vessel segment, takes place at vessel bifurcations. The fractional flow of erythrocytes into one daughter branch, FQ_{rbc} is calculated from the respective fractional blood flow, FQ_B as follows (Pries *et al.*, 1989)

$$\text{logit}\left(FQ_{rbc2}\right)=A+B\text{logit}\left(\frac{FQ_{B2}-X_0}{1-2X_0}\right) \quad (9)$$

where logit x=ln[x/(1-x)] and the parameters A, B, and X_0 defining the phase separation characteristics of bifurcation of the experimental study in the rat mesentery by Pries *et al.* (1989). The parameters are expressed as

$$A=-13.29\frac{(D_2/D_3)^2-1}{(D_2/D_3)^2+1}\frac{1-H_{D_1}}{D_1} \quad (10)$$

$$B=1+6.98\frac{1-H_{D_1}}{D_1} \quad (11)$$

$$X_0=0.964\frac{1-H_{D_1}}{D_1} \quad (12)$$

where subscript *1*, *2* and *3* are the parent vessel and the daughter branches, respectively. Subsequently, hematocrit in the daughter vessels is calculated according to

$$HD_2 = FQ_{rbc2}.H_{D1}.Q_1/Q_2 \quad (13)$$

where Q_1 and Q_2 are the flowrate in the parent and daughter vessel, respectively.

Low frequency flow ($\omega\rightarrow 0$); The input impedance of zero angular frequency for any vessel segment is analogous to the DC impedance in the electrical terminology or the resistance in Poiseuille equation (Olufsen, 1998; Huo and Kassab, 2006). This can be obtained by letting $\omega\rightarrow 0$ in Equation 1:

$$\begin{aligned}Z(0,0)&=\lim_{\omega\to 0}Z(0,\omega)\\&=\lim_{\omega\to 0}\frac{ig^{-1}\sin(\omega L/c)+Z(L,\omega)\cos(\omega L/c)}{\cos(\omega L/c)+igZ(L,\omega)\sin(\omega L/c)}\\&=\frac{8\mu L}{\pi a^4}+Z(L,0)\end{aligned} \quad (14)$$

where L and a are the length and radius of vessel segments, respectively; ω is the angular frequency; $Z(0,0)$ and $Z(L,0)$ are the impedance at entrance and exit of the vessel segment respectively; and μ is the blood viscosity. The equation suggests that as the angular frequency approaches zero, pulsatile flow can be approximated using steady flow.

2.3 Boundary conditions

Two types of outlet boundary conditions were tested at the terminal vessels of the arterial trees, which are also the end nodes of the pre-capillary arterioles. The first type uses an finite impedance that is identified from the steady circulation analysis of the network model. The impedances represent resistance of blood flow in the capillary and veinal vasculatures. The second type is a zero impedance boundary condition. For the zero impedance, flowrate and pressure amplitudes

are zero at the outlet boundaries.

Mouse heart beat, f was taken as 500 beat/min (angular frequency, ω is 52.36 rad/s). A constant blood viscosity of 4.9cP (according to Windberger *et al.* (2003) at hematocrit and shear rate of 0.4 and 94s^{-1}, respectively) and Young modulus (E) of 0.5MPa were used.

A mean pressure of 40mmHg and a single harmonic pressure of 5(cosωt) mmHg with zero phase angle were applied at the inlet node of the artery. The value of 5 for the amplitude of oscillation is approximated based on the findings of Intaglietta *et al.* (1971).

2.4 Method of solution

Computation of impedance; Knowing the radius of the vessel segment, a, length of vessel segment, L, oscillation angular frequency, ω, density of blood, ρ, viscosity of blood, μ, vessel wall thickness, h, and Young's modulus of the vessel segment, E, parameters such as c, F_J, w, C and g in Equations 1 to 5 can be calculated for each vessel segment in the vascular network. The computation starts from the end node of the pre-capillary arterioles and proceeds progressively to the root of the arterial tree. The outlet impedance, $Z_{daug}(L,\omega)$ at the end of pre-capillary arterioles is given as the boundary conditions. Subsequently, the impedance at the beginning of the pre-capillary arterioles, $Z_{daug}(0,\omega)$ can be found using Equation 1. In vascular network, two pre-capillary arterioles arise from a parent vessel. The impedance at bifurcation (or impedance at the end of the parent vessel, i.e., the load impedance $Z_{par}(L,\omega)$ of the parent vessel) is found using

$$\frac{1}{Z(L,\omega)_{par}} = \frac{1}{Z(0,\omega)_{daug1}} + \frac{1}{Z(0,\omega)_{daug2}} \quad (15)$$

Equation 14 is given under the assumption that the flow is conserved and the pressure is continuous at vascular bifurcation. The computations are repeated to the root of vasculature of the arterial tree in recursive manner (backward marching) progressively.

Computation of pressure and flowrate; In a reversed manner to the impedance computation, pressure and flowrate are calculated from the root vessel segment to the pre-capillary arterioles using the calculated input impedance, $Z(0,\omega)$ and load impedance, $Z(L,\omega)$ at the nodes of a vessel segment.

Computation of steady calculation; Steady flow calculations are carried out using the low frequency ($\omega \rightarrow 0$) formulation and by specifying pressure at the inlet of the arterial tree as 40mmHg. Impedance, nodal pressure and segmental flowrate are calculated using backward marching and forward marching computations. For the case of zero outlet boundary condition, the steady pressure of 0mmHg is specified at the end node of the pre-capillary arterioles.

Computation of in vivo viscosity; In vivo viscosity in the vessel segments of the arterial trees was calculated using the low frequency $(\omega \rightarrow 0)$ formulation and by specifying *HD* of 0.45 at the inlet vessel segment of the arterial trees. There are six inlets for the six arterial trees. The computation begins by marching backwards to calculate the impedance and then marching forwards to calculate pressure and flowrate. Since the flowrate in each of the parent and daughter vessels is known, hematocrit and *in vivo* viscosity can be calculated in the daughter vessels using Equation 6. The backward and forward marching computations are carried out iteratively until the change of the input impedance of the vessel segments in the arterial trees is less than 0.1%.

2.5 Simulations

Four groups of simulations were carried out: (i) S1: constant viscosity (4.9cP) with the outlet impedance boundary condition determined from the steady circulation analysis (ii) S2: constant viscosity with zero outlet impedance boundary condition; (iii) S3: as S1 but with *in vivo* viscosity; and (iv) S4: as S2 but with *in vivo* viscosity.

3 Results and Discussion

3.1 Input Impedance

The normalised pulsatile flow and pressure waves at the inlet of the arterial tree are given in Figure 2. In case S1, the amplitude of flowrate is amplified and the phase is shifted with respect to the pressure wave. The peak of the normalised flowrate precedes the peak of the normalised input pressure, which indicates that the vasculatures behave as a compliant system. Much more data for the inlet nodes and vessel segments as stated in Figure 1b are given in Table 1. The inlet pulsatile pressure, which peaks at 0.12s, is used as a reference wave to determine phase shift.

3.2 Constant and *in vivo* viscosities

The steady flowrate at the inlets is $241.69\text{x}10^{-14}\text{m}^3/\text{s}$ and $257.23\text{x}10^{-14}\text{m}^3/\text{s}$ for case S1 and case S3, respectively (Node 1a; Table 1). The flowrate is lower in S1 because the resistance of the arterial tree is higher for the constant viscosity (0.0049cP) than for the *in vivo* viscosity. The amplitude of normalised pulsatile flowrate and phase shift are higher for S3 than for S1 (Figure 2), which is due to an increase of the *in vivo* viscosity in the arterioles at periphery. Such increases can be noted by referring to the viscosity in the vessel segments of 1a, 2b, 3c, 4d and 5e, which are 0.026, 0.031, 0.038, 0.051 and 0.069cP, respectively.

3.3 Zero and non-zero outlet impedance

Case S2 does not incorporate capillary and veinal vasculatures and a pressure of 0mmHg is specified at the terminals of the arterial tree. This makes the resistance of A1 for case S1 higher than for case S2, which can be inferred from inlet steady flowrate (e.g., steady flowrate is $241.69\text{x}10^{-14}\text{m}^3/\text{s}$ and $393.02\text{x}10^{-14}\text{m}^3/\text{s}$ for S1 and S2, respectively, in Table 1). It is interesting to note that the amplitude of normalised pulsatile flowrate and phase shift of S1 is greater than that of S2 although the inlet flowrate is much greater in S2. Besides, the arterial trees behave lesser compliantly in the cases of zero outlet impedance (S2 and S4) than in the cases of non-zero outlet impedance condition (S1 and S3). Such results show that the capillary and veinal vasculatures play a significance role towards dynamic response of the oscillating pressure and flowrate in the arterial vasculature. The approach with a zero outlet impedance boundary condition obviously has a different dynamic response at the inlet of arterial trees from that with a non-zero outlet impedance boundary condition.

It appears that the impedance of the capillary vasculature produces a reflection to the characteristic waves, which increases the amplitude of the normalised pulsatile flowrate and pressure waveform as the waves travel from the inlet to the terminal vessel of the arterial tree. The increase of amplitude further dilates the nearest pre-capillary arterioles and temporally increases pressure drop between the pre-capillary arterioles and capillaries. If, however, the capillaries resistance remain unchanged, the reflected wave is transmitted to the higher parent vessels. Therefore, the compliant nature of the arterial trees plays a crucial role in determining the characteristics of the flow. For pathological conditions such as arteriosclerosis, the vessels in the arterial trees become less compliant leading to changes in the dynamic response of oscillating pressure and flowrate.

3.4 Frequency of oscillation

The dependency of the input impedance at the inlet of the arterial tree on angular frequencies has been investigated. At zero or near zero angular frequency ($\omega \rightarrow 0$), the oscillating impedance is equal to the steady input impedance, which is described by Equation 14, and the phase shift of the oscillating impedance is zero. In Figure 3, the ratio of the oscillating input impedance, $|Z_{inlet}(0,\omega)|$ at the inlet of A1 over steady input impedance of S1 is plotted versus angular frequencies for the cases S1, S2, S3 and S4. In general, the oscillating input impedance and the phase shift angle decreases as the frequency increases.

The heart beat of mouse ranges from 300 to 500 beat/min (or 31 to 55 rad/s) and for such angular frequencies, there is a significant reduction in the oscillating input impedance and an increase in phase shift for case S1 (or S3) in Figure 3. Unlike the case S1 (or S3), the angular frequency has a small effect on the oscillating input impedance in case S2 (or S4). The prediction of the oscillating input impedances for cases S1 and S2 are quite close beyond 100 rad/s and such a condition is similar to cases S3 and S4. The change of the oscillating input impedance beyond 300 rad/s is very small. At higher frequencies, especially beyond 300 rad/s, the phase shift of the oscillating input impendence of the arterial trees settled at a single value, which is about -45 and -50 degree for the constant viscosity (cases S1 and S2) and in vivo viscosity (cases S3 and S4), respectively.

3.5 Young's Modulus, E

The dependency of oscillating input impedance at the inlet of the arterial tree on E values has been investigated for S1, S2, S3 and S4. Angular frequency was fixed as 52.36 rad/s. In Figure 4, the ratio of the oscillating input impedance, $|Z_{inlet}(0,\omega)|$ at the inlet of A1 over the steady input impedance of S1 is plotted versus E values for cases S1, S2, S3 and S4. In general, the oscillating input impedance reduces as the value of E reduces (Figure 4). A compliance vessel reduces the oscillating input impedance of blood flow in a network.

The reduction of the oscillating input impedance of cases S1 and S3 starts at E value $1x10^7$ Pa (Figure 4). In the cases of a zero outlet boundary condition (S2 and S4), the value of E of the vessel segments must be less than $2x10^6$ Pa in order to bring changes to the oscillating input impedance and therefore, suggesting that capillary and veinal vasculature play a role in lowering oscillating input impedance in much harder vessels.

4 Conclusion

A model has been developed to simulate pulsatile flow in mouse retinal vasculatures. The features of the present work are; 1) The use of a finite load impedance at the terminal vessel of the arterial trees. The load impedance was determined from a steady circulation analysis of a very detailed network model, which includes capillary and veinal vasculatures of the mouse. The load impedance represents the true impedance of the blood flow in the capillary and veinal vasculatures; 2) The use of an appropriate *in vivo* viscosity in the mice retinal vessels obtained from Pries et al. (1989, 1994) mathematical models. The viscosity includes the uneven distribution of erythrocyte at bifurcation and description of *in vivo* viscosity, which consider the role of endothelium surface layer (ESL);

The outcomes of the present work are; 1) The flowrate at the inlet of the arterial trees responded in a different manner for the non-zero and the zero outlet impedance conditions; 2) The frequency of heart beat and the elasticity of vessels play a crucial role in lowering oscillation input impedance. At the angular frequency near to the heart beat of human (6 to 10 rad/s), oscillating input impedance is found to reduce for cases S1 and S3; 3) The presence of capillary and veinal vasculatures reduces the oscillating input impedance of the arterial tree.

The critiques of the model are; 1) The Womersley solution mathematical model does not incorporate nonlinear advective losses, but the size of mice retinal vessels are small and such assumption is not expected to introduce significant uncertainties; 2) The evaluation of *in vivo* viscosity is based on steady flowrate. 3) The information on the retinal vessel wall properties is very limited and insufficient. In future studies, the present model will be extended to represent the entire retinal circuit of arterial and veinal trees and capillary vasculature. Future studies are also required to determine the mechanical properties of the retinal vessel *in vivo*.

References

Atabek, H., Lew, H., 1966. Wave propagation through a viscous incompressible fluid contained in an initially stressed elastic tube. Biophys. J. 8, 626–649.

Attinger, E. O., 1964. Pulsatile Blood Flow. New York, McGraw-Hill.

Balarathnasingam, C., Morgan, W.H., Hazelton, M.L., et al., 2007. Value of retinal vein pulsation characteristics in predicting increased optic disc excavation. Br. J. Opthalmol. 91, 441–4.

Feke, G.T., Goger, D.G., Tagawa, H., Delori, F.C., 1987. Laser Doppler technique for absolute measurement of blood speed in retinal vessels. IEEE Trans. Biomed. Eng. 34, 673–680.

Frash, H.F., Kresh, J.Y., Noordergraaf, A., 1944. Wave transmission and input impedance of a model of skeletal muscle microvasculature. Ann. Biomed. Eng. 22, 45-47.

Gaehtgens, P.A., 1970. Pulsatile pressure and flow in the mesenteric vascular bed of the cat. Arch. Ges. Phyisol.,316, 462-473.

Ganesan, P., He, S., Xu, H., 2009. Network modeling of vasculature and circulation of mouse retina. Submitted to the Microvas. Res.

Huo, Y., Kassab, G.S., 2006. Pulsatile blood flow in the entire coronary arterial tree: theory and experiment. Am. J. Physiol. Heart Circ. Physiol. 291, 1074-1087.

Levine, D.N., 1998. Spontaneous pulsation of the retinal veins. Microvasc. Res. 56, 154–165.

McDonald, D. A., 1960. Blood Flow in Arteries. Baltimore, Williams and Wilkins.

Olufsen, M.S., C.S. Peskin, W.Y. Kim, E.M. Pedersen, Nadim A., and Larsen J. 2000. Numerical simulation and experimental validation of blood flow in arteries with structured-tree outflow conditions, Ann. Biomed. Eng. 28, 1281–1299.

Pedley, T.J., 1980. The Fluid Mechanics of Large Blood Vessels. Cambridge: Cambridge University Press, 1–159.

Pries, A.R, Ley, K., Claassen, K.L., Gaehtgens P., 1989. Red cell distribtion at microvascular bifurcation. Microvas. Res. 38, 81-101.

Pries, A.R., Secomb, T.W., Gross, J.F, Gaehtgens, P., 1994. Blood flow in microvascular networks. Experiments and simulation. Cir. Res. 67, 904-915.

Pries A.R, Secomb T.W., GeBner, Sperandio M.B, Gross J.F, Gaehtgens, Resistance to blood flow in microvessels *in vivo*, Cir. Res. 1994;75: 904-915.

Riva, C.E., Petrig, B., 1980. Blue field entoptic phenomenon and blood velocity in the retinal capillaries. J. Opt. Soc. Am. 70, 1234–1238.

White, B., 2003. *In vivo* dynamic human retinal blood flow imaging using ultra-high-speed spectral domain optical coherence tomography. Opt. Express 11, 3490–3497.

Zamir, M., 2005. The physics of coronary blood flow. Springer, USA.

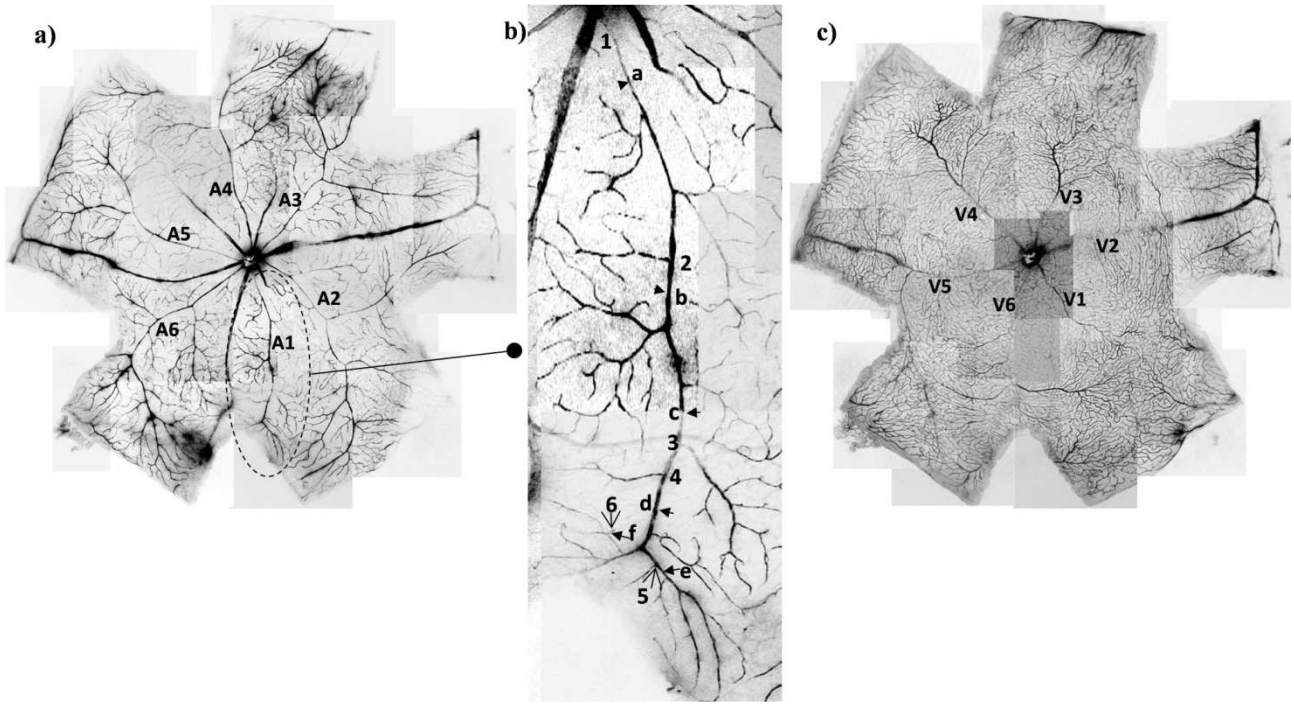

Figure 1: Network topologies of the mouse retina; a) superficial layer; b) arterial tree A1; c) deep layer.

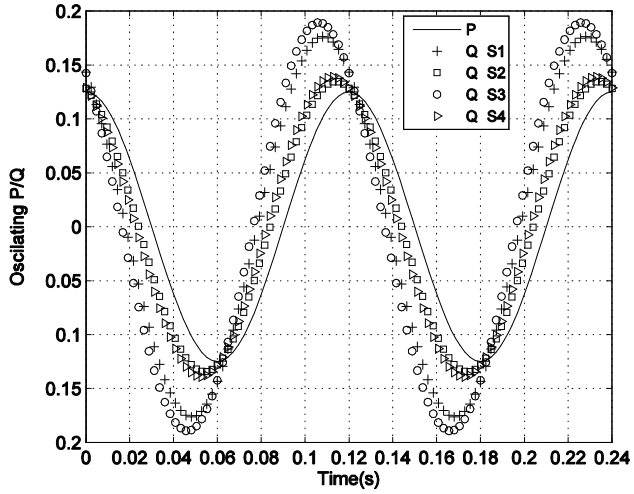

Figure 2: Normalised pressure and flowrate waveforms against it steady component at the inlet of A1.

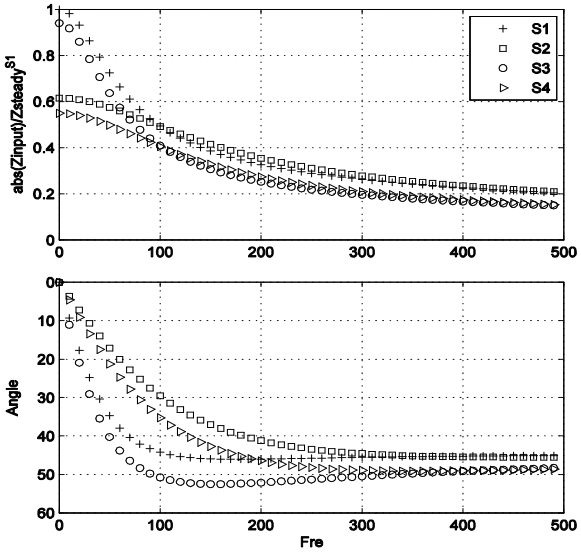

Figure 3: Normalised |Zinlet|/Zsteady$_{S1}$ (top) and phase angle (bottom) at the inlet of A1 versus angular frequencies.

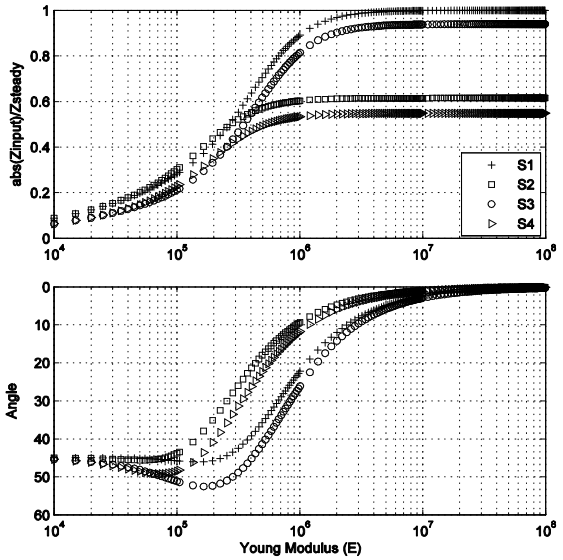

Figure 4: Normalised oscillating input impedance |Zinlet|/Zsteady$_{S1}$ (top) and phase angle (bottom) at the inlet of A1 versus Young's modulus (E).

Table 1: Pressure (P), flowrate (Q) and wall shear stress (WSS) for nodes and vessels specified in Figure 1b.

Nodes	Dia	Vis	HD	Steady component			ratio (Oscillating / Steady)					
				Nodal P	Q (1x10^{-14})	WSS	P		Q		WSS	
	(μm)	(Poise)		(mmHg)	(m^3/s)	(Pa)	Amp	Phase	Amp	Phase	Amp	Phase
						S1						
1a	22.635	0.0049	0.450	40.000	241.695	10.358	0.125	0.00	0.176	35.56	0.176	-144.43
2b	19.827	0.0049	0.450	28.004	127.190	8.110	0.163	14.56	0.201	44.35	0.201	-135.64
3c	16.112	0.0049	0.450	21.380	52.192	6.202	0.200	28.77	0.232	55.37	0.232	-124.63
4d	13.164	0.0049	0.450	20.187	26.758	5.829	0.208	31.83	0.242	58.69	0.242	-121.30
5e	9.832	0.0049	0.450	16.436	6.642	3.472	0.237	44.96	0.288	76.85	0.288	-103.15
6f	5.750	0.0049	0.450	12.988	2.215	5.789	0.233	52.70	0.233	52.70	0.233	-127.30
						S2						
1a	22.635	0.0049	0.450	40.000	393.017	16.843	0.125	0.00	0.135	17.84	0.135	-162.16
2b	19.827	0.0049	0.450	20.572	203.397	12.968	0.135	13.54	0.137	22.00	0.137	-158.00
3c	16.112	0.0049	0.450	10.247	75.352	8.954	0.138	21.33	0.138	25.75	0.138	-154.24
4d	13.164	0.0049	0.450	8.765	34.577	7.532	0.138	22.74	0.139	27.24	0.139	-152.76
5e	9.832	0.0049	0.450	3.864	9.038	4.725	0.139	26.36	0.139	28.81	0.139	-151.19
6f	5.750	0.0049	0.450	0.000	3.113	8.138	0	0	0	0	0	0
						S3						
1a	22.635	0.0026	0.450	40.000	257.228	5.830	0.125	0.00	0.189	41.19	0.189	-138.80
2b	19.827	0.0031	0.497	32.885	138.333	5.631	0.170	16.07	0.221	50.78	0.221	-129.21
3c	16.112	0.0038	0.514	27.664	59.474	5.505	0.219	32.95	0.262	62.28	0.262	-117.72
4d	13.164	0.0051	0.553	26.432	29.593	6.754	0.229	36.63	0.277	66.54	0.277	-113.46
5e	9.832	0.0069	0.556	21.651	7.592	5.587	0.270	52.07	0.335	84.50	0.335	-95.50
6f	5.750	0.0095	0.531	14.136	2.410	12.285	0.265	60.41	0.265	60.41	0.265	-119.59
						S4						
1a	22.635	0.0026	0.450	40.000	440.376	9.980	0.125	0.00	0.139	22.11	0.139	-157.89
2b	19.827	0.0031	0.497	27.764	237.908	9.689	0.138	14.41	0.144	27.70	0.144	-152.29
3c	16.112	0.0038	0.512	18.684	101.201	9.325	0.145	25.13	0.147	32.66	0.147	-147.34
4d	13.164	0.0049	0.538	16.912	45.678	9.937	0.146	27.24	0.148	35.53	0.148	-144.47
5e	9.832	0.0069	0.558	9.788	12.436	9.196	0.148	33.77	0.149	38.84	0.149	-141.16
6f	5.750	0.0102	0.566	0.000	4.020	21.874	0	0	0	0	0	0